IEEE Access
Multidisciplinary | Rapid Review | Open Access Journal

Received May 27, 2019, accepted June 11, 2019, date of publication June 28, 2019, date of current version July 18, 2019.

Digital Object Identifier 10.1109/ACCESS.2019.2925701

Virtual Full-Duplex Distributed Spatial Modulation: A New Protocol for Cooperative Diversity

AMIR SHEHNI, (Student Member, IEEE), AND MARK F. FLANAGAN, (Senior Member, IEEE)
School of Electrical and Electronic Engineering, University College Dublin, Dublin, D04 V1W8 Ireland

Corresponding author: Amir Shehni (amir.shehni@ucdconnect.ie)

This work was supported by the Science Foundation Ireland under Grant 13/CDA/2199.

ABSTRACT Spatial modulation, a multi-antenna technology which uses the antenna index as an additional means of conveying information, is an emerging technology for modern wireless communications. In this paper, a new distributed version of spatial modulation is proposed which achieves *virtual* full-duplex communication (VFD-DSM) in order to increase system throughput. This throughput improvement is achieved by allowing the source to transmit new data while the relays *implicitly* forward the source's data in every time slot (via the index of the active relay) while *explicitly* transmitting their own data (via a conventional modulation technique). Motivated by the achievable throughput improvement with VFD-DSM, two maximum *a posteriori* (MAP) detection methods are proposed for implementation at the destination node: the first, called *local MAP*, is based on processing the signals received over two or three consecutive time slots, while the second, called *global MAP*, is based on symbol-error-rate optimal detection over an entire frame of data. For each MAP detection method, an *error-aware* version of the detector is also proposed which takes into account the demodulation error rate at the relays; this can achieve an extra BER advantage at the cost of additional complexity and an increased channel state information (CSI) requirement. Simulation results demonstrate that the proposed VFD-DSM protocol can provide an improved BER compared to the baseline protocol of successive relaying, while also providing a significant increase in the overall throughput since the relays can forward the source symbols while simultaneously transmitting their own data. The proposed VFD-DSM detectors are shown to provide a range of design choices offering different tradeoffs between BER performance and computational complexity. Finally, the impact of the data frame length in VFD-DSM on the error rate performance and system throughput is investigated, and it is shown how to choose the optimal frame length for a given target system throughput.

INDEX TERMS Spatial modulation, full-duplex communication, relay networks, forward-backward algorithm.

I. INTRODUCTION

Multiple-input multiple-output (MIMO) systems, which use multiple antenna resources at the transmitter and receiver of a wireless communication system, have attracted significant attention in the research community over the last two decades, mainly due to their excellent advantages such as the ability to leverage diversity gain and spatial multiplexing gain [1]. However, in spite of the many advantages of MIMO systems, there are some practical issues which arise from the use of multiple antennas, which are related to the system complexity and cost. These problems mainly stem from the need to implement multiple RF chains (one for each antenna), which causes issues related to inter-channel interference (ICI) and inter-antenna synchronization (IAS) [2], [3].

Spatial modulation (SM) has been proposed as a new modulation technique for MIMO communication, which requires only a *single* RF chain at the transmitter. This has the advantage of reducing the cost and complexity of the system while still maintaining many of the benefits of MIMO [4]. The key idea is that in SM, only *one* antenna is active (or transmitting) in any particular time slot, and the *choice* of active antenna (i.e., the antenna *index*) conveys information in addition to that conveyed by the conventional (IQ-domain) symbol [2]–[6].

The principle of SM was extended to the scenario of half-duplex cooperative networks in [7]–[12]. In particular,

The associate editor coordinating the review of this manuscript and approving it for publication was Kwok L. Chung.

a *distributed* spatial modulation (DSM) protocol was proposed in [10], [11]; here, the relay which becomes active in the seond (cooperative) phase of communication is that which corresponds to the source symbol transmitted in the first (broadcast) phase. The use of DSM therefore increases the total network throughput, since the relays transmit their own data in the conventional IQ-domain while the *index* of the activated relay conveys additional information regarding the source data. The DSM protocol is particularly suitable for uplink communication, where SM becomes difficult to implement due to the lack of multiple transmit antennas at the transmitter of a mobile device. Here the DSM system can use distributed cooperative half-duplex relays to form a virtual MIMO system. However, despite the benefits of DSM over other distributed cooperation protocols, the use of cooperation limits the source data throughput to $1/2$ symbol per channel use (i.e., it is the same as that of conventional relay networks).

Full-duplex communication in cooperative networks has been studied in [13] and [18], where the source and relays transmit data in every time slot, thus doubling the throughput of the system compared to the case of half-duplex cooperation (e.g., those proposed in [19]–[22]). Here the relays can be equipped with multiple antennas, but the existence of *self-interference* is a significant problem to be solved. One solution is to consider a distributed version of the half-duplex system, called *virtual full-duplex* (VFD), where the transmit and receive antennas belong to physically separated nodes [23], [24].

Motivated by the performance advantages of full-duplex communication, in this paper, a new virtual full-duplex protocol is proposed based on the principle of DSM. This new protocol achieves a significant throughput improvement compared to conventional half-duplex DSM. Two detection methods are also proposed for implementation at the destination node. The first detection method, called *local* MAP detection, applies the MAP detection principle over two or three consecutive time slots and requires feedforward of previous decisions. The second detection method, called *global* MAP detection, is symbol-error-rate optimal and is based on the forward-backward algorithm (also known as the Bahl-Cocke-Jelinek-Raviv algorithm, after the authors of the first paper on this topic [25]). A description of this VFD-DSM protocol was presented earlier in [26]; however, the present paper provides a number of significant extensions with respect to the work in [26]: (i) the local MAP detector in [26] is extended to three time slots, allowing the system to achieve a significant gain in the BER performance; (ii) for all proposed detection methods at the destination, robust (''error-aware'') detectors are also derived which take into the account the probability of demodulation error at the relays; (iii) the impact of frame length on both error rate and system throughput is analysed, and it is shown how to choose the frame length to optimize the error performance for a given target system throughput; and (iv) a comprehensive comparison is presented of the error rate performance and computational complexity of all proposed detectors, as well as the robustness of the VFD-DSM protocol to variations in the channel geometry.

Note that a virtual full-duplex DSM protocol was also proposed in [27]. This protocol used an additional relay, called a *proxy relay*, which is activated if and only if it receives two successive equal symbols from the source. It was shown in [27] that this protocol exhibits a similar BER performance versus the SNR-per-bit compared to the baseline full-duplex protocol of *successive relaying* [28]- [32]; however, the addition of the proxy relay increases the complexity and cost of the system. In contrast to that work, here the same data throughput is achieved without the need for an extra relay.

The remainder of this paper is organized as follows. In Section II, the system model and the proposed VFD-DSM protocol are described. In Section III, the two proposed detectors at the destination are derived, based on the local and global application of the MAP principle. In Section IV, the corresponding error-aware detectors are developed. Section V discusses system design considerations (frame length, complexity of algorithms, etc.) and presents simulation results. Finally, conclusions are drawn in Section VI.

II. SYSTEM MODEL

A. A BRIEF REVIEW OF DISTRIBUTED SPATIAL MODULATION

This section provides a brief overview of the operation of the conventional half-duplex DSM protocol [10], [11]. Here the network topology is comprised of a single source, a single destination, and $M_s = 2^q$ relays. A fixed unique q-bit digital identifier (ID) is assigned to each relay. Two time slots are required for a complete transmission; in the first time slot, the source broadcasts an M_s-ary symbol; this is received by the destination and is also received and demodulated by all relays. In the second time slot, if the demodulated source data at any relay matches that relay's ID, the relay will become active and transmit its own data to the destination (using a conventional modulation format). Fig. 1 A) shows an illustrative example of DSM for the case $M_s = 2$. Thus, the signal received by the destination from the activated relay conveys information regarding the source data (through the relay-to-destination channel coefficient) as well as the relay's data. The destination's received signals for these two consecutive time slots are jointly processed at the destination (based on the MAP detection principle) in order to jointly detect the source data for the first time slot and the relay data for the second time slot.

B. PROPOSED VIRTUAL FULL-DUPLEX DSM PROTOCOL

In this section, we describe the proposed DSM protocol, which extends the protocol described in the previous subsection to achieve virtual full-duplex communication. This is a *frame-based* communication protocol; a frame of $N + 1$ time slots is used to transmit N source symbols. The relay activation rule is the same as in the previous subsection; however, here a new symbol is transmitted by the source in

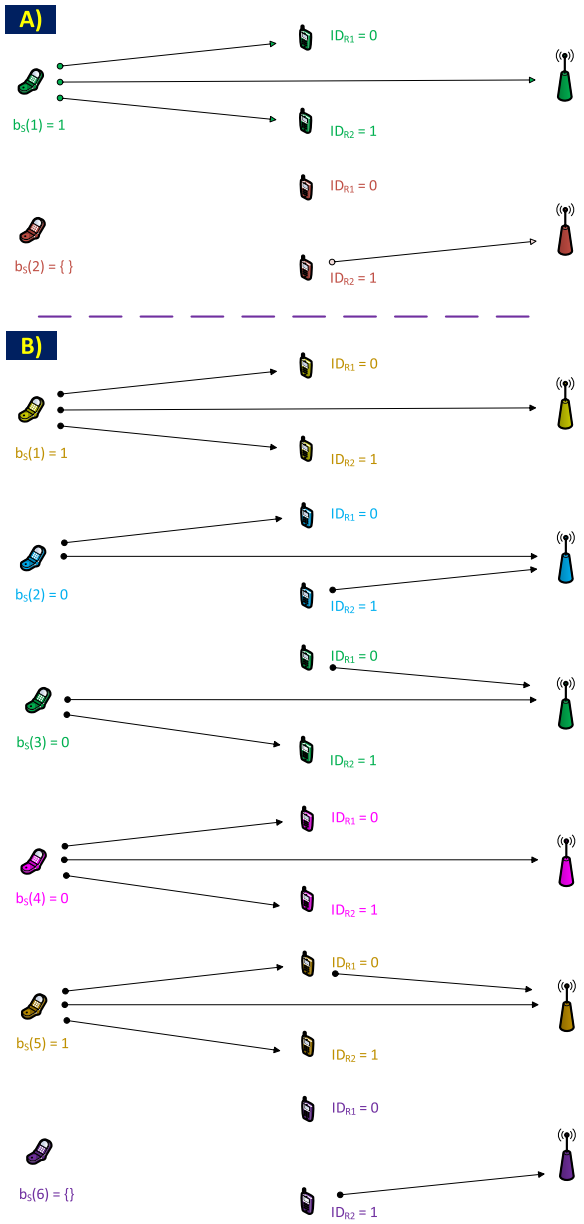

FIGURE 1. A) Illustration of distributed spatial modulation (DSM) for the case $M_s = 2$. In the first time slot, the source broadcasts its data-bearing symbol; in the second time slot, the relay whose ID matches the received source data will become active and transmit its own data-bearing symbol to the destination. B) An illustration of virtual full-duplex DSM for the case $N = 5$ and $M_s = 2$. Here the source data sequence is $\{b_s(1), b_s(2), b_s(3), b_s(4), b_s(5)\} = \{1, 0, 0, 0, 1\}$ (terminated by a time slot during which the source is silent). For ease of exposition, it is assumed that no demodulation errors occur at the relays.

every time slot k, where $1 \leq k \leq N$. In time slot $N + 1$, the source is silent, or equivalently transmits the constellation symbol 0 which is not "detected" by the destination. Fig. 1 B) illustrates the operation of the proposed virtual full-duplex DSM protocol. The illustration is for the case of $M_s = 2$ relays with digital identifiers $\mathrm{ID}_{R_1} = 0$ and $\mathrm{ID}_{R_2} = 1$. The source data sequence of length $N = 5$ is given by $\{b_s(1), b_s(2), b_s(3), b_s(4), b_s(5)\} = \{1, 0, 0, 0, 1\}$. For ease of exposition, it is assumed for this example that no demodulation errors occur at the relays.

At first glance, the fact that the source transmits in every time slot can be seen to cause a potential problem regarding the destination's detection procedure. It will regularly occur that the source broadcasts two or more successive equal symbols, as occurs for example in time slots 2, 3, and 4 in Fig. 1B) (i.e., $b_s(2) = b_s(3) = b_s(4) = 0$). This means that relay R_1, whose ID matches this symbol, will miss its activation in time slot 4, as it is active in time slot 3 and therefore cannot detect the source symbol $b_s(3)$. However, the key observation here is that the resulting silence (inactivation) of all relays in time slot 4 *also conveys information*; therefore, this event does not cause any problem provided that the destination's MAP detector is aware of this event and takes it into account as one of the hypotheses during its MAP detection procedure. Explicit details regarding how this is achieved will be given in the next section.

C. DEFINITIONS AND NOTATIONS

We will adopt the following definitions and notations throughout this paper. A network topology consisting of a single source (S), a single destination (D), and $M_s = 2^q$ relays $\{R_1, R_2, \ldots, R_{M_s}\}$ is assumed. Each node is equipped with a single antenna, and every relay (as well as the source) has its own data to be communicated to the destination. The source uses phase shift keying (PSK) or quadrature amplitude modulation (QAM) signaling, where the complex constellation is denoted by $\mathcal{A}_s$. It is assumed that this constellation is normalized to have unit average energy, i.e., $\mathbb{E}_{x\in\mathcal{A}_s}\{|x|^2\} = 1$. The symbol transmitted by the source in time slot $k \geq 1$ is $x_s(k) = \mathcal{M}_s(\mathbf{b}_s(k))$, where $\mathbf{b}_s(k)$ is the information bit vector of length $\log_2(M_s)$ and $\mathcal{M}_s(.)$ represents the bit-to-symbol mapping at the source. Similarly, each relay F which is active in time slot $k > 1$ uses a unit-energy PSK/QAM constellation $\mathcal{A}_r$ of size M_r to transmit its own data-bearing symbol $x_F(k) = \mathcal{M}_r(\mathbf{b}_F(k))$, where $\mathbf{b}_F(k)$ is the information bit vector of relay F having length $\log_2(M_r)$, and $\mathcal{M}_r(.)$ represents the bit-to-symbol mapping at relay F.

We denote the received signal at any node B in time slot k by $y_B(k)$. The noise component of this signal is denoted by $n_B(k)$ – this has a mean of zero and a variance of $\sigma^2 = N_0/2$ per dimension, where N_0 denotes the noise power spectral density. Denote by h_{XY} the fading channel coefficient between nodes X and Y – this is a circularly symmetric complex Gaussian random variable having a mean of zero and a variance of σ^2_{XY} (*i.e.*, all channels are assumed to exhibit Rayleigh fading). Channel coefficients for different links and/or different time slots are assumed to be independent and identically distributed (i.i.d.). The set of active relays in time slot $k \geq 1$ is denoted by $\Phi_k \subseteq \{R_1, R_2, \ldots, R_{M_s}\}$ and its complement $\bar{\Phi}_k$ represents the set of inactive (or silent) relays – note that these relays will be in receive mode in time slot k. Since no relay is active in the first time slot, the initialization $\Phi_1 = \emptyset$ holds. Finally, each relay has a unique digital identifier ID_{R_r} for $r = 1, 2, \ldots, M_s$ which is

a vector of $\log_2(M_s)$ bits. Throughout this paper, vectors are denoted by bold type.

D. SIGNAL TRANSMISSION AND RELAY ACTIVATION

1) SOURCE BROADCASTING AND RELAY DETECTION

In the proposed VFD-DSM communication protocol, the source broadcasts a new data-bearing symbol in every time slot. Therefore, in each time slot $k \geq 1$ every inactive relay $F \in \bar{\Phi}_k$ receives from the source the signal

$$y_F(k) = \sqrt{E_s} h_{SF}(k) x_s(k) + n_F(k) \,, \tag{1}$$

where E_s denotes the average transmit energy per symbol at the source. Note that here we have neglected the effect of inter-relay interference (IRI). Each relay $F \in \bar{\Phi}_k$ then demodulates according to the MAP criterion, yielding the source symbol estimate

$$\hat{x}_s^{(F)}(k) = \underset{\tilde{x}_s(k) \in \mathcal{A}_s}{\arg\min} \{ |y_F(k) - \sqrt{E_s} h_{SF}(k) \tilde{x}_s(k)|^2 \} \tag{2}$$

and relay $F \in \bar{\Phi}_k$ then correspondingly estimates the source data via $\hat{b}_s^{(F)}(k) = \mathcal{M}_s^{-1}(\hat{x}_s^{(F)}(k))$.

2) RELAY ACTIVATION MECHANISM

In each time slot, the SM encoding principle is applied to the set of M_s distributed relays in order to *implicitly* forward the estimate of the source data and to *explicitly* transmit the activated relay's own data. Each relay F which demodulated a symbol in a particular time slot k compares its source data estimate $\hat{b}_S^{(F)}(k)$ with its own unique ID; if there is a match, relay F will become active in time slot $k+1$. Of course, if relay F is already active in time slot k, it cannot receive and demodulate the source data as it is in the process of transmitting, so it must be silent in time slot $k+1$. Therefore, the activation rule can be summarized mathematically as

$F \in \Phi_{k+1}$ if and only if $F \in \bar{\Phi}_k$ *and* $\hat{b}_s^{(F)}(k) = \mathrm{ID}_F$.

III. DESTINATION PROCESSING: LOCAL MAP AND GLOBAL MAP DETECTION

In this section, we propose two detection techniques for implementation at the destination node. The first, called *local MAP detection*, works by processing two or three consecutive received signals, utilising feedforward of detection decisions from previous time slots. The second, called *global MAP detection*, uses the forward-backward algorithm to determine the exact *a posteriori* probabilities (APPs) of the source symbols *and* the relay symbols conditioned on the *entire frame* of $N+1$ received signals. Thus, global MAP detection minimizes the achievable symbol error rate.

Note that it may occur that more than one relay, or indeed no relay, might be active in a particular time slot, as demodulation errors may occur at the relays. However, in this section, the detection algorithm implemented at the destination will assume that the demodulation of the source symbols at each relay is error-free. The extension of these detection algorithms to the case where demodulation errors exist at the relays will be described in detail in Section IV.

A. LOCAL MAP DETECTION

1) LOCAL MAP DETECTION OVER TWO TIME SLOTS (2TS)

The received signal at the destination in the previous time slot $k-1$ (which was stored at the destination for processing in the current time slot) may be written as (3), as shown at the bottom of this page, while the received signal at the destination in the current time slot k may be written as (4), as shown at the bottom of this page. In these expressions, E_r denotes the average transmit symbol energy at each relay.

According to the DSM principle, the source data in time slot $k-1$ is communicated to the destination in two ways. First, it is directly modulated onto the symbol $x_s(k-1)$; and second, it controls the set Φ_k of active relays in time slot k (including the case where $\Phi_k = \emptyset$). Therefore, joint MAP detection can be applied at the destination over the two time slots $k-1$ and k conditioned on the two received signals $y_D(k-1)$ and $y_D(k)$ given by (3) and (4) respectively; here the MAP detector will consider all hypotheses regarding the previous and current source symbols $x_s(k-1)$ and $x_s(k)$, the current active relay set Φ_k, and the corresponding relays' data symbols. Therefore, the destination's detection process for local MAP operates according to (5), as shown at the bottom of this page, and the detected data is obtained via $\hat{b}_s(k-1) = \mathcal{M}_s^{-1}(\hat{x}_s(k-1))$ and $\hat{b}_G(k) = \mathcal{M}_r^{-1}(\hat{x}_G(k))$ for every $G \in \hat{\Phi}_k$. Note that $\tilde{x}_s(k-1)$ and $\tilde{x}_s(k)$ represent hypotheses for the source data in time slots $k-1$ and k, respectively. In addition, $\tilde{\Phi}_k$ denotes the hypothesized active relay set,

$$y_D(k-1) = \sqrt{E_s} h_{SD}(k-1) x_s(k-1) + \sum_{J \in \Phi_{k-1}} \sqrt{E_r} h_{JD}(k-1) x_J(k-1) + n_D(k-1). \tag{3}$$

$$y_D(k) = \sqrt{E_s} h_{SD}(k) x_s(k) + \sum_{G \in \Phi_k} \sqrt{E_r} h_{GD}(k) x_G(k) + n_D(k). \tag{4}$$

$$\left\{ \hat{x}_s(k-1), \hat{\Phi}_k, \{\hat{x}_G(k)\} \right\} = \underset{\substack{\tilde{x}_s(k-1), \tilde{x}_s(k) \in \mathcal{A}_s \\ \tilde{x}_G(k) \in \mathcal{A}_r \forall G \in \tilde{\Phi}_k}}{\arg\min} \left\{ \left| y_D(k-1) - \left(\sqrt{E_s} h_{SD}(k-1) \tilde{x}_s(k-1) + \textstyle\sum_{J \in \hat{\Phi}_{k-1}} \sqrt{E_r} h_{JD}(k-1) \hat{x}_J(k-1) \right) \right|^2 \right.$$
$$\left. + \left| y_D(k) - \left(\sqrt{E_s} h_{SD}(k) \tilde{x}_s(k) + \textstyle\sum_{G \in \tilde{\Phi}_k} \sqrt{E_r} h_{GD}(k) \tilde{x}_G(k) \right) \right|^2 \right\}. \tag{5}$$

while $\tilde{x}_G(k)$ represents a hypothesis for the transmitted data of any relay G which is hypothesized to be active in time slot k (i.e., $G \in \tilde{\Phi}_k$). Finally, note that in order to ensure that the detection procedure yields a result consistent with the relay activation conditions of VFD-DSM, we impose the following constraint on the source symbol and active relay set hypotheses: $F \in \tilde{\Phi}_k$ if and only if $F \notin \hat{\Phi}_{k-1}$ and $\tilde{b}_s^{(F)}(k-1) = \mathrm{ID}_F$; we also initialize $\hat{\Phi}_1 = \emptyset$.

Note that this detector provides the joint MAP decision conditioned on the two consecutive received signals $y_D(k-1)$ and $y_D(k)$, based on the assumption that the decisions made in previous time slots are correct. Also note that the termination of each frame with a zero symbol mitigates against the effect of error propagation.

2) LOCAL MAP DETECTION OVER THREE TIME SLOTS (3TS)

It is straightforward to extend the detection procedure described in the previous subsection to the case of local MAP detection over three consecutive time slots. This makes the detector more robust (especially to the condition where the source transmits two consecutive equal symbols, leading to all relays being silent in the third time slot), at the expense of a higher computational complexity. The destination's detector performs joint MAP detection over the three time slots k, $k-1, k-2$ conditioned on the received signals (4), (3) and (6), as shown at the bottom of this page.

The MAP detector considers all hypotheses regarding the source symbols $x_s(k-2), x_s(k-1)$ and $x_s(k)$, the previous and current active relay sets Φ_{k-1} and Φ_k, and the corresponding relays' data symbols. Therefore, the destination's detection process operates according to (7), as shown at the bottom of this page, and the detected data is obtained via $\hat{b}_s(k-2) = \mathcal{M}_s^{-1}(\hat{x}_s(k-2))$ and $\hat{b}_J(k-1) = \mathcal{M}_r^{-1}(\hat{x}_J(k-1))$ for every $J \in \hat{\Phi}_{k-1}$. Note that $\tilde{x}_s(k-2)$, $\tilde{x}_s(k-1)$ and $\tilde{x}_s(k)$ represent hypotheses for the source data in time slots $k-2$, $k-1$ and k respectively, while the previous decisions on the active relay set $\hat{\Phi}_{k-2}$ and its associated transmissions $\hat{x}_L(k-2)$ (for $L \in \hat{\Phi}_{k-2}$) are assumed to be correct. In addition, $\tilde{\Phi}_{k-1}$ and $\tilde{\Phi}_k$ denote the hypothesized active relay sets, while $\tilde{x}_J(k-1)$ and $\tilde{x}_G(k)$ represent the associated transmit symbol hypotheses. Finally, we impose the following constraints on the considered hypotheses: (i) $F \in \tilde{\Phi}_{k-1}$ if and only if $F \notin \hat{\Phi}_{k-2}$ and $\tilde{b}_s^{(F)}(k-2) = \mathrm{ID}_F$, and (ii) $F \in \tilde{\Phi}_k$ if and only if $F \notin \tilde{\Phi}_{k-1}$ and $\tilde{b}_s^{(F)}(k-1) = \mathrm{ID}_F$; we also initialize $\hat{\Phi}_1 = \emptyset$. Again, the frame termination with a zero symbol guards against the adverse effect of error propagation.

B. GLOBAL MAP DETECTION

In this section, we describe the detector at the destination which is based on the application of the MAP detection principle at a global (i.e., frame) level. This detector efficiently computes the APPs of the source and relay symbols by using the forward-backward algorithm on the factor graph which describes the joint probability distribution of these random variables. This type of detector was originally proposed for soft decoding of convolutional codes in [25], and is known as the BCJR algorithm after the initials of the authors of [25]. This approach was later significantly generalized in [33], where it was shown how to apply the forward-backward algorithm to compute exact APPs for any context where the factor graph describing the global probability distribution is a tree.

Here we apply the forward-backward algorithm to the context of VFD-DSM, noting that the computation of the APPs for a single transmission frame may be formulated as the problem of marginalizing a product of functions. The factor graph for the overall probability distribution relating to the detection problem is shown in Fig. 2; note that this factor graph is a tree. The messages passed on the factor graph are also shown in Fig. 2; the message passed on each edge of the graph is a function of the variable node connected to that edge. Each variable node $x_s(k)$ corresponds to the source symbol (lying in $\mathcal{A}_s$) in time slot k, while each variable node $\mathbf{x}_R(k) = [x_{R_1}(k)\ x_{R_2}(k)\ \cdots\ x_{R_{M_s}}(k)]$ corresponds to the *relay*

$$y_D(k-2) = \sqrt{E_s}\, h_{SD}(k-2)\, x_s(k-2) + \sum_{L \in \Phi_{k-2}} \sqrt{E_r}\, h_{LD}(k-2)\, x_L(k-2) + n_D(k-2). \tag{6}$$

$$\begin{aligned}
&\left\{\hat{x}_s(k-2),\, \hat{\Phi}_{k-1},\, \{\hat{x}_J(k-1)\}\right\} \\
&= \underset{\substack{\tilde{x}_s(k-2),\tilde{x}_s(k-1),\tilde{x}_s(k) \in \mathcal{A}_s \\ \tilde{x}_J(k-1),\tilde{x}_G(k) \in \mathcal{A}_r \forall J \in \tilde{\Phi}_{k-1}, G \in \tilde{\Phi}_k}}{\arg\min} \left\{ \left| y_D(k-2) - \left(\sqrt{E_s} h_{SD}(k-2) \tilde{x}_s(k-2) + \sum_{L \in \hat{\Phi}_{k-2}} \sqrt{E_r} h_{LD}(k-2) \hat{x}_L(k-2) \right) \right|^2 \right. \\
&\quad + \left| y_D(k-1) - \left(\sqrt{E_s} h_{SD}(k-1) \tilde{x}_s(k-1) + \sum_{J \in \tilde{\Phi}_{k-1}} \sqrt{E_r} h_{JD}(k-1) \hat{x}_J(k-1) \right) \right|^2 \\
&\quad \left. + \left| y_D(k) - \left(\sqrt{E_s} h_{SD}(k) \tilde{x}_s(k) + \sum_{G \in \tilde{\Phi}_k} \sqrt{E_r} h_{GD}(k) \tilde{x}_G(k) \right) \right|^2 \right\}.
\end{aligned} \tag{7}$$

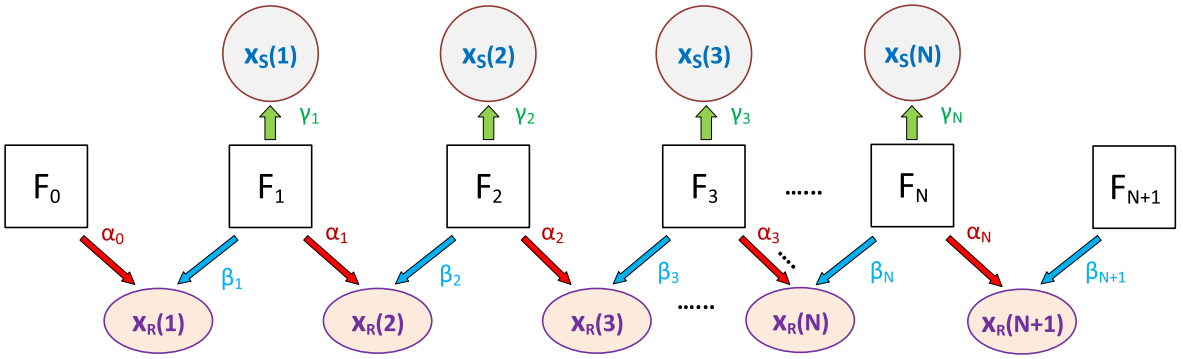

FIGURE 2. Illustration of the factor graph and associated message passing (forward-backward) algorithm for global MAP detection in VFD-DSM. The red arrows show the propagation of the forward recursion (α metrics), and the blue arrows indicate the backward recursion (β metrics).

transmission vector (lying in the Cartesian product $\mathcal{A}_r^M$) in time slot k. Each factor node F_k (for $1 \le k \le N$) represents the function given by (8) and $p\big(y_D(k) \mid x_S(k), \mathbf{x}_R(k)\big)$ is given by (9), both as shown at the bottom of this page, and $\mathbf{h}_{RD}(k) = [h_{R_1 D}(k)\ h_{R_2 D}(k)\ \cdots\ h_{R_{M_s} D}(k)]$. Note that the term $p\big(\mathbf{x}_R(k+1) \mid x_S(k), \mathbf{x}_R(k)\big)$ expresses the probabilistic dependency of the next relay transmission vector on the current relay transmission vector and the current source symbol (due to the relay activation principle of the proposed VFD-DSM protocol). This coupling is what creates the tree structure in the factor graph in Fig. 2. If the demodulation process at the relays is assumed to be error-free, the probability distribution $p\big(\mathbf{x}_R(k+1) \mid x_S(k), \mathbf{x}_R(k)\big)$ can be assumed to be uniform over all relay symbol vectors $\mathbf{x}_R(k+1)$ which are consistent with the hypotheses $x_S(k)$ and $\mathbf{x}_R(k)$.

The forward-backward algorithm begins with the (simultaneous) recursive computation of the forward metrics α_k and the backward metrics β_k [33]. For the forward recursion, the initialization for the forward metrics is given by

$$\alpha_0\big(\mathbf{x}_R(1)\big) = F_0 = p\big(\mathbf{x}_R(1)\big) = \begin{cases} 1; & \text{if } \mathbf{x}_R(1) = \mathbf{0} \\ 0; & \text{otherwise} \end{cases}, \tag{10}$$

and the recursion operates as follows: for every $k = 1, 2, \ldots, N$,

$$\alpha_k\big(\mathbf{x}_R(k+1)\big) = \sum_{x_s(k)} \sum_{\mathbf{x}_R(k)} F_k\big(x_S(k), \mathbf{x}_R(k), \mathbf{x}_R(k+1)\big) \times \alpha_{k-1}\big(\mathbf{x}_R(k)\big). \tag{11}$$

The initialization for the backward metrics is given by (12), as shown at the top of the next page and the recursion operates as follows: for every $k = N, N-1, \ldots, 1$,

$$\beta_k\ (\mathbf{x}_R(k)) = \sum_{x_S(k)} \sum_{\mathbf{x}_R(k+1)} F_k\big(x_S(k), \mathbf{x}_R(k), \mathbf{x}_R(k+1)\big) \times \cdot\ \beta_{k+1}\big(\mathbf{x}_R(k+1)\big). \tag{13}$$

Finally, the metrics γ_k are computed for every $k = 1, 2, \ldots, N$ via

$$\gamma_k\big(x_S(k)\big) = \sum_{\mathbf{x}_R(k)} \sum_{\mathbf{x}_R(k+1)} F_k\big(x_S(k), \mathbf{x}_R(k), \mathbf{x}_R(k+1)\big) \times \alpha_{k-1}\big(\mathbf{x}_R(k)\big) \cdot\ \beta_{k+1}\big(\mathbf{x}_R(k+1)\big). \tag{14}$$

Note that for any value of k, the values of $\gamma_k(x_S(k))$ correspond to the exact APPs of the source symbols $x_S(k)$. Decisions on the source symbols are then made via

$$\hat{x}_s^{(D)}(k) = \arg\max_{x_S(k)}\ \gamma_k\big(x_S(k)\big). \tag{15}$$

Simultaneously with the γ_k metric computation, the metrics δ_k are computed via

$$\delta_k(\mathbf{x}_R(k)) = \alpha_{k-1}(\mathbf{x}_R(k))\ \beta_k(\mathbf{x}_R(k)) \tag{16}$$

for each $k = 2, 3, \ldots, N+1$. Note that this requires only one multiplication for each value of $\mathbf{x}_R(k)$. For any value of k, the values of $\delta_k(\mathbf{x}_R(k))$ correspond to the exact APPs of the relay symbol vectors $\mathbf{x}_R(k)$. Decisions on the relay symbol vectors are then made via

$$\hat{\mathbf{x}}_R(k) = \arg\max_{\mathbf{x}_R(k)} \delta_k(\mathbf{x}_R(k)). \tag{17}$$

Here the termination of the frame with a zero symbol facilitates the initialization of the backward recursion via (12). Also, log-domain metric computation is recommended for implementation of this algorithm, as for the standard BCJR algorithm of [25]; in such an implementation, all metrics are replaced by their real logarithms, multiplication is replaced by addition, and addition is replaced by the well-known Jacobian logarithm (max*) [34], defined by

$$\max^*\{x, y\} = \log(e^x + e^y) \tag{18}$$

$$= \max\{x, y\} + \log\left(1 + e^{-|x-y|}\right). \tag{19}$$

$$F_k\ (x_S(k), \mathbf{x}_R(k), \mathbf{x}_R(k+1)) = p\ (y_D(k) \,|\, x_S(k), \mathbf{x}_R(k)) \cdot p\ (\mathbf{x}_R(k+1) \,|\, x_S(k), \mathbf{x}_R(k))\ . \tag{8}$$

$$p\ (y_D(k) \mid x_S(k), \mathbf{x}_R(k)) = \frac{1}{\pi N_0} \exp\left[-\frac{\left| y_D(k) - \sqrt{E_s} h_{SD}(k) x_S(k) - \sqrt{E_r} \mathbf{h}_{RD}^T(k) \mathbf{x}_R(k) \right|^2}{N_0} \right]. \tag{9}$$

$$\beta_{N+1}\big(\mathbf{x}_R(N+1)\big)=F_{N+1}=p\big(y_D(N+1)\mid \mathbf{x}_R(N+1)\big)=\frac{1}{\pi N_0}\exp\left[-\frac{\left|y_D(N+1)-\sqrt{E_r}\mathbf{h}_{RD}^T(N+1)\mathbf{x}_R(N+1)\right|^2}{N_0}\right]. \quad (12)$$

Note that in implementation of the Jacobian logarithm, the omission of the second term in (19) causes only a minor loss in performance.

IV. DESTINATION PROCESSING: ERROR-AWARE DEMODULATORS

The local and global MAP detectors introduced in the previous sections assumed error-free detection of the source symbols at the relays. This assumption will not hold in general, especially at low source-relay SNR. Motivated by this consideration, in this section we introduce detectors which are robust in the presence of demodulation errors at the relays, in a manner similar to the work of [35] and [36].

A. ERROR-AWARE LOCAL MAP

For brevity, we consider only the local MAP demodulator which processes over three time slots. This demodulator seeks to detect the most likely source symbols in time slots $k-2, k-1, k$, relay activations in time slot $k-1$ and k, *and* relay transmitted symbols in time slots $k-1$ and k in a joint manner (while retaining the past decisions on the active relays and their transmitted symbols in time slot $k-2$). Therefore, the MAP demodulator seeks to maximize

$$P_D = P\Big(\tilde{x}_s(k-2),\tilde{x}_s(k-1),\tilde{x}_s(k),\tilde{\mathbf{x}}_R(k-1),\tilde{\mathbf{x}}_R(k)\mid\ y_D(k-2),y_D(k-1),y_D(k)\Big) \quad (20)$$

where $\tilde{\mathbf{x}}_R(j)$ denotes a hypothesis for the *vector* of symbols transmitted from the relays in time slot $j\in\{k-1,k\}$. Applying Bayes' rule, factorizing, and ignoring constants, leads to the detection procedure given by (21), as shown at the bottom of this page.

Next we explain how to compute the term

$$P\left(\tilde{\mathbf{x}}_R(k)\mid\tilde{x}_s(k-1),\tilde{\mathbf{x}}_R(k-1)\right), \quad (22)$$

which appears in (21). First, the symbol error probability at relay $F\in\Phi$ in time slot k is in general given by an expression of the form

$$P_{e,b}^{(F)}(k)=\beta Q\left(\sqrt{2\alpha\ |h_{SF}(k)|^2(E_s/N_0)}\right) \quad (23)$$

where α and β are constants depending on the particular (PSK or QAM) modulation used at the source.

We can factorize (22) as

$$P\big(\tilde{\mathbf{x}}_R(k)\mid\tilde{x}_s(k-1),\hat{\mathbf{x}}_R(k-1)\big) = \prod_{F\in\widetilde{\Phi}_{k-1}^{(\mathrm{ON})}} P(\tilde{x}_F(k)\mid\tilde{x}_s(k-1),\hat{x}_F(k-1)) \times \prod_{F\in\widetilde{\Phi}_{k-1}^{(\mathrm{OFF})}} P(\tilde{x}_F(k)\mid\tilde{x}_s(k-1),\hat{x}_F(k-1)), \quad (24)$$

where $\widetilde{\Phi}_{k-1}^{(\mathrm{ON})}$ represents the set of relays which are *active* based on the relay symbol vector hypothesis $\tilde{\mathbf{p}}_R(k-1)$ and $\widetilde{\Phi}_{k-1}^{(\mathrm{OFF})}$ represents the set of relays which are *inactive* based on $\tilde{\mathbf{p}}_R(k-1)$. Next, for $F\in\widetilde{\Phi}_k^{(\mathrm{ON})}$ we have

$$P(\tilde{x}_F(k)\mid\tilde{x}_s(k-1),\hat{x}_F(k-1)) = \begin{cases} 0 & \text{if } \hat{p}_F(k-1)\neq 0 \\ \frac{1}{N}(1-P_e^{(F)}) & \text{if } \hat{x}_F(k-1)=0 \text{ and } \tilde{x}_s(k-1)=\mathrm{ID}_F \\ \frac{1}{N}P_e^{(F)} & \text{otherwise,}\end{cases} \quad (25)$$

and for $F\in\widetilde{\Phi}_{k-1}^{(\mathrm{OFF})}$,

$$P(\tilde{x}_F(k)\mid\tilde{x}_s(k-1),\hat{x}_F(k-1)) = \begin{cases} 1 & \text{if } \hat{x}_F(k-1)\neq 0 \\ P_e^{(F)} & \text{if } \hat{x}_F(k-1)=0 \text{ and } \tilde{x}_s(k-1)=\mathrm{ID}_F \\ 1-P_e^{(F)} & \text{otherwise.}\end{cases} \quad (26)$$

$$\begin{aligned}\left\{\hat{x}_s(k-2),\hat{\mathbf{x}}_R(k-1)\right\} = \underset{\substack{\tilde{x}_s(k-2),\tilde{x}_s(k-1),\tilde{x}_s(k)\in\mathcal{A}_s\\ \tilde{x}_J(k-1),\tilde{x}_G(k)\in\mathcal{A}_r\,\forall J\in\tilde{\Phi}_{k-1},G\in\tilde{\Phi}_k}}{\arg\min} \Bigg\{ &\left|y_D(k-2)-\left(\sqrt{E_s}h_{SD}(k-2)\tilde{x}_s(k-2)+\sum_{L\in\hat{\Phi}_{k-2}}\sqrt{E_r}h_{LD}(k-2)\hat{x}_L(k-2)\right)\right|^2 \\ &+\left|y_D(k-1)-\left(\sqrt{E_s}h_{SD}(k-1)\tilde{x}_s(k-1)+\sum_{J\in\tilde{\Phi}_{k-1}}\sqrt{E_r}h_{JD}(k-1)\hat{x}_J(k-1)\right)\right|^2 - N_0\log P\left(\tilde{\mathbf{x}}_R(k-1)\mid\tilde{x}_s(k-2),\hat{\mathbf{x}}_R(k-2)\right) \\ &+\left|y_D(k)-\left(\sqrt{E_s}h_{SD}(k)\tilde{x}_s(k)+\sum_{G\in\tilde{\Phi}_k}\sqrt{E_r}h_{GD}(k)\,\tilde{x}_G(k)\right)\right|^2 - N_0\log P\left(\tilde{\mathbf{x}}_R(k)\mid\tilde{x}_s(k-1),\tilde{\mathbf{x}}_R(k-1)\right)\Bigg\}. \end{aligned} \quad (21)$$

The first case in (25) and (26) corresponds to the case where relay F was busy in the previous time slot, and hence cannot be active in the current time slot. The second case in (25) corresponds to the probability of *correct activation* of relay F, where the relay has been silent in previous time slot and has been able to check the received source symbol against its own ID. The third case in (25) is the probability of *incorrect activation*. The term $\frac{1}{N}$ in (25) is also due to the fact that when any relay is active, its transmitted symbols are equiprobable. The second case in (26) corresponds to the probability of *incorrect non-activation* where the relay has been able to receive the new source data but demodulates such data incorrectly, and the third case corresponds to the probability of *correct non-activation*.

The error-aware local MAP detector is then determined by substituting the expressions given by (25) and (26) into (20).

B. ERROR-AWARE GLOBAL MAP

The derivation of a robust MAP demodulator for VFD-DSM, it is only necessary to evaluate the term $p\big(\mathbf{x}_R(k+1) \mid x_S(k), \mathbf{x}_R(k)\big)$ in (8). However, this has already been explained in the previous section.

V. DESIGN CONSIDERATIONS AND SIMULATION RESULTS

In this section, simulation results are presented and some design considerations are investigated such as choice of frame length N and detection complexity. In addition, a state-of-the-art full-duplex cooperative relaying protocol, called *successive relaying* [28]– [32] is considered as a baseline for performance comparison. In successive relaying, in each time slot exactly one relay is receiving a new symbol from the source, while at the same time the other relay is forwarding the symbol received from the source in the previous time slot to the destination (the relays alterate their roles between transmission and reception). A direct link is also assumed to exist betweeen the source and the destination. It should be noted that in successive relaying, the relays do not have their own data to be communicated; they simply retransmit the source data to the destination. The destination performs MAP detection over two consecutive time slots in a fashion similar to the local MAP detector. In order to have a fair comparison, both error-aware and low-complexity demodulators are considered for successive relaying. A node geometry is considered which assumes an equal distance between all pairs of nodes, i.e., $\sigma^2_{SD} = \sigma^2_{SR_r} = \sigma^2_{R_rD} = 1$ for $r = 1, 2$. Also, unless otherwise specified we set $E_s = E_r$.

A. IMPACT OF FRAME LENGTH

Recall that the proposed protocol operates on the basis of a frame consisting of $N + 1$ time slots. As we will show in this section, it is important to choose an appropriate value of N. A large value of N can have drawbacks which differ depending on the particular receiver algorithm used. In the case of global MAP detection, a large N means the use of a large memory buffer at the receiver, as the detection algorithm

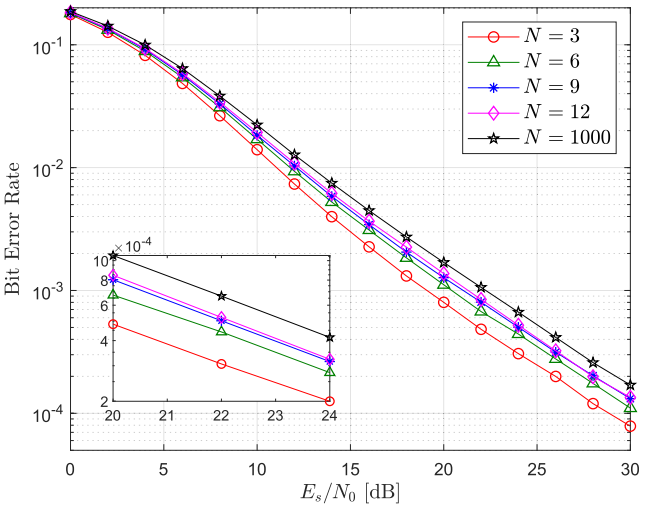

FIGURE 3. BER for the source data at the destination for the proposed VFD-DSM scheme with local MAP detection (over 3 time slots), for different frame lengths.

requires storage of the entire trellis of length $N + 1$. In the case of local MAP detection, a large value of N increases the effect of an error propagation event within a frame (local MAP detection is predicated on the assumption that previous symbol decisions in the frame are correct; however, the effect of an error propagation event must terminate at the end of the frame).

The impact of frame length on the source data BER performance for both local MAP detection (over 3 time slots) and global MAP detection is shown in Fig. 3 and Fig. 4 respectively. As can be seen, for local MAP detection, the system using frame length 3 has 2.2dB gain over the system with frame length 12 and 3dB gain over the system with frame length 1000. This is due to the suppression of the error propagation effect at short frame lengths. A similar trend in the variation of the source data BER performance with N can be observed in Fig. 4 for the case of global MAP detection. Here, the reason is that smaller N means more frequent frame termination with the source transmitting a zero symbol; this in turn leads to frequent strong backward-metric initialization in the forward-backward algorithm.

On the other hand, it is important to note that choosing too low a frame length will adversely affect the throughput of the system, especially if N is very small. In the proposed VFD-DSM protocol, in the first time slot, while the source broadcasts its symbol, there is no cooperative transmission from the relays. On the other hand, in the final time slot, although the relays make a cooperative transmission, there is no transmission from the source. Therefore, a total of $N + 1$ time slots is required for transmission of N source symbols as well as (on average) $1 + \frac{M_s-1}{M_s}(N-1)$ relay symbols (note that in the second time slot, one relay will be active, whereas in the following time slots, one relay will be active *only* if the new source symbol is not equal to the previous source symbol, which occurs with probability $\frac{M_s-1}{M_s}$).

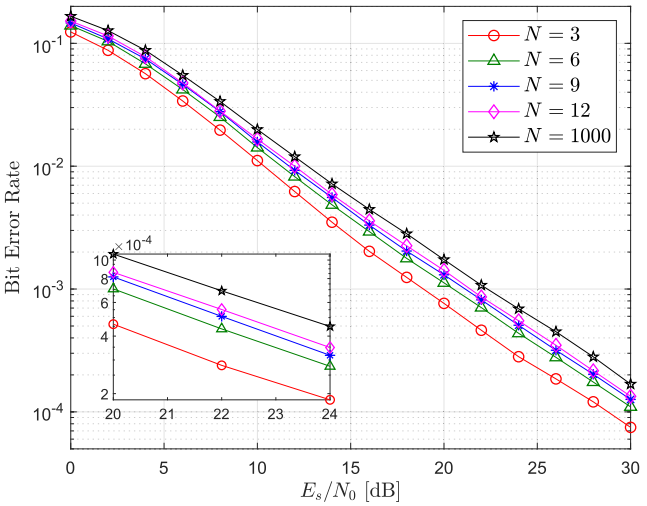

FIGURE 4. BER for the source data at the destination for the proposed VFD-DSM scheme with global MAP detection, for different frame lengths.

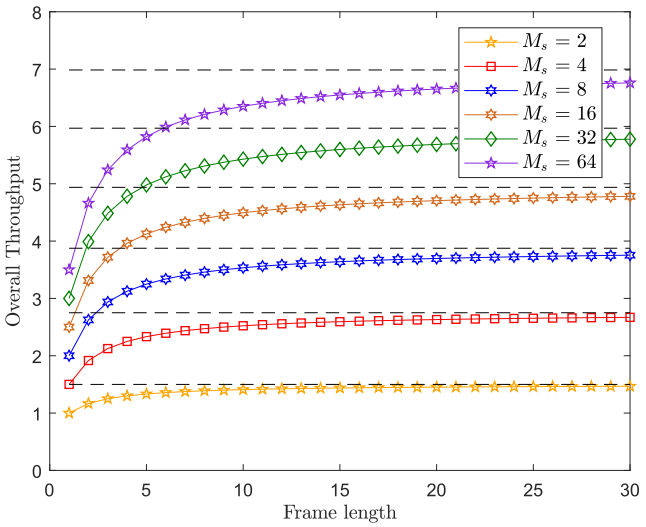

FIGURE 5. Variation of the system throughput with frame length N, shown for different source constellation size M_s. Here BPSK is used at the relays ($M_r = 2$).

Therefore, the total transmitted energy per frame is

$$E_{\text{tot}} = N \cdot E_s + \left[1 + \frac{M_s - 1}{M_s}(N-1)\right] E_r. \tag{27}$$

Similarly, the total number of (source and relay) bits transmitted per frame is

$$B_{\text{tot}} = N \cdot \log_2 M_s + \left[1 + \frac{M_s - 1}{M_s}(N-1)\right] \log_2 M_r. \tag{28}$$

The energy per bit is $E_b = E_{\text{tot}}/B_{\text{tot}}$. Note that in the case $E_s = E_r = E$ and $M_s = M_r = M$, this evaluates to $E_b = E/(\log_2 M)$, as expected. The throughput of the system, measured in bits per time slot, is given by

$$T = \frac{B_{\text{tot}}}{N+1} = \frac{N}{N+1}\log_2 M_s + \left[\frac{1}{N+1} + \left(\frac{M_s - 1}{M_s}\right)\left(\frac{N-1}{N+1}\right)\right] \log_2 M_r. \tag{29}$$

As $N \to \infty$, the throughput tends to the asymptotic value

$$T_\infty = \log_2 M_s + \log_2 M_r \left(\frac{M_s - 1}{M_s}\right). \tag{30}$$

Fig. 5 illustrates the behavior of the overall system throughput with frame length N and different source constellation size $M_s \in \{2, 4, 8, 16, 32, 64\}$, for the case where the relays use BPSK signaling ($M_r = 2$). The asymptotic throughput values T_∞ are also shown. It can be seen that for reasonable-sized frame length N, the throughput is close to its asymptotic value, but it decays dramatically as N becomes small.

In practice, it is desirable to choose a value of N which provides a compromise between throughput, algorithmic storage requirements, and performance. As a design principle, one may choose to target a certain fraction η of the asymptotic throughput, and the optimal frame length can then be determined as the smallest N which satisfies this throughput requirement. For example, for the case of $M_s = M_r = 2$ and $\eta = 94.5\%$, we require $T \geq \eta T_\infty = 1.423$; the optimal frame length is then $N = 12$ as shown in Fig. 5. This choice of frame length provides close-to-maximum throughput while it is also memory-efficient and provides close to optimal BER performance as shown in Fig. 3 and 4.

B. COMPUTATIONAL COMPLEXITY ANALYSIS OF PROPOSED DETECTORS FOR VFD-DSM

A comparison of the computational complexity of the proposed detectors for use at the destination in VFD-DSM is presented in Table 1. The low-complexity (LC) and error-aware (EA) demodulators have been listed in the table, as well as an *approximate error-aware* (AEA) demodulator. The latter represents the situations in which for the larger values of M_s, the complexity of the demodulator can be dramatically reduced by restricting the set of hypothesized vectors to those for which $\left|\widetilde{\Phi}^{(\text{ON})}\right| \leq 2$. This assumption leads to very little loss in performance, since the probability of more than 2 simultaneous relay activations is negligible at reasonable values of the source-relay SNR. Table 1 expresses the computational complexity of each detector in big-O notation in order to show how this complexity scales with the constellation sizes M_s and M_r (full details regarding the derivations of these expressions are omitted due to space constraints). Note that while the global MAP detector exhibits a lower computational complexity to the local MAP detector (3TS) in general, it incurs a significantly higher computational storage requirement (which scales linearly with the frame length N). For the purpose of comparison, the complexity of the detectors for successive relaying are also shown in the table.

C. RESULTS

In this section, simulation results are presented for the proposed VFD-DSM protocol, considering all proposed destination detectors (local MAP with 2 and with 3 time slots, global MAP) and also considering the low-complexity and

TABLE 1. Complexity of the destination's detection mechanism for the proposed VFD-DSM protocols.

Protocol	Low-complexity (LC)	Error-aware (EA)	Approximate error-aware (AEA)
Successive relaying	$O\left(M_s^2\right)$	$O\left(M_s^3\right)$	–
Local MAP (2TS)	$O\left(M_s^2 M_r\right)$	$O\left(M_s^2 M_r^{M_s}\right)$	$O\left(M_s^4 M_r^2\right)$
Local MAP (3TS)	$O\left(M_s^3 M_r^2\right)$	$O\left(M_s^3 M_r^{2M_s}\right)$	$O\left(M_s^7 M_r^4\right)$
Global MAP	$O\left(M_s^3 M_r^2\right)$	$O\left(M_s M_r^{2M_s}\right)$	$O\left(M_s^5 M_r^4\right)$

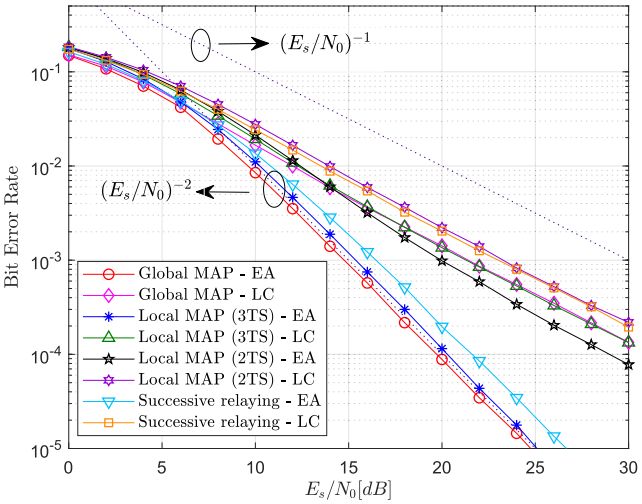

FIGURE 6. BER of the source data at the destination, for the proposed local and global MAP detectors (over 2 and 3 time slots) for the proposed VFD-DSM protocol. Both the low-complexity and error-aware demodulators are used for detection. It is assumed that BPSK is employed at both source and relays. The frame length is chosen to be $N = 12$.

error-aware versions of the proposed demodulators. The results are also compared to the state-of-the-art full-duplex relaying protocol of successive relaying (for the purpose of fair comparison, results are presented for both low-complexity and error-aware demodulators for successive relaying). Simulations assume a system with 2 relays, with BPSK employed at both source and relays ($M_s = M_r = 2$). The frame length is chosen as $N = 12$, based on the optimization discussed in the previous section. Inter-relay interference is neglected in this work.

A comparison of the bit error rate (BER) for the source data at the destination for the proposed VFD-DSM protocol and successive relaying is shown in Fig. 6. First we will consider the performance of the low-complexity (LC) demodulators in Fig. 6. It can be seen that at high SNR, VFD-DSM with local MAP detection (2TS) has a very similar BER performance to that of successive relaying (attaining a BER of 10^{-3} at $E_s/N_0 = 24$ dB), but attains a clear throughput advantage since in VFD-DSM the relays are able to simultaneously transmit their own data. It can also be seen from the figure that the use of local MAP detection (3TS) and global MAP detection both exhibit a further gain of approximately 2dB in the source data BER.

Next we consider the performance of the error-aware (EA) demodulators shown in Fig. 6. In this case, it can be seen that VFD-DSM with local MAP detection (3TS) achieves a gain of 1.1 dB over successive relaying at a BER of 10^{-3}, and when global MAP detection is used, an additional 0.6 dB is gained. All three of these demodulators achieve diversity order 2. On the other hand, local MAP detection (2TS) does not achieve any diversity gain. In general, the use of the error-aware demodulators leads to an improved BER performance for full-duplex relaying systems; this comes at the expense of an increased detection complexity as well as the assumption of perfect knowledge of the source-to-relay channel coefficients at the destination. Note that apart from the benefit in the source data BER, the proposed VFD-DSM protocol also possesses a clear superiority over successive relaying in the sense of improved system data rate (since in VFD-DSM, the relay nodes also transmit their own data). The reason for this is that while the energy used in the relay nodes is for the purpose of relay data transmission, it also provides an independent copy of the source symbol via the DSM principle, thus providing source symbol diversity and improving the source data BER.

In VFD-DSM (and indeed DSM), the relays cannot achieve any diversity gain for their own data; they simply aid the source transmissions if and only if they can simultaneously serve their own traffic. The BER performance of the relay data at the destination for the proposed destination detectors is shown in Fig. 7. It may be seen from the figure that for all systems, the best performance is obtained with error-aware (EA) detection. In this context, the proposed VFD-DSM with local MAP detection (3TS) and with global MAP detection exhibit a similar performance; both show a gain of 2.5 dB over VFD-DSM with local MAP detection (2TS). A similar comparative performance can also be seen in the case where the low-complexity (LC) detector is employed. It should be noted that in VFD-DSM the relay nodes transmit their *own* data, while in successive relaying all relay resources are committed *only* to serving the source data; this explains the absence of any curve in Fig. 7 for successive relaying.

Fig. 8 shows the BER of the source data for the case of 4 relays, where QPSK is used at the source and BPSK is used at the relays ($M_s = 4$, $M_r = 2$). Here the low-complexity demodulator is chosen for detection in each case. It can be seen that in this scenario, the VFD-DSM protocol with local

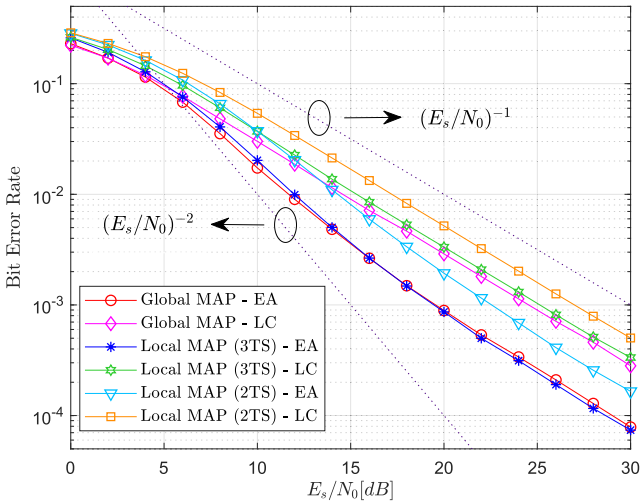

FIGURE 7. BER of the relay data at the destination, for the proposed VFD-DSM protocol with local MAP detection (over 2 and 3 time slots) as well as global MAP detection. Both the low-complexity and error-aware demodulators are used for detection. It is assumed that BPSK is used at both source and relays. The frame length is chosen to be $N = 12$.

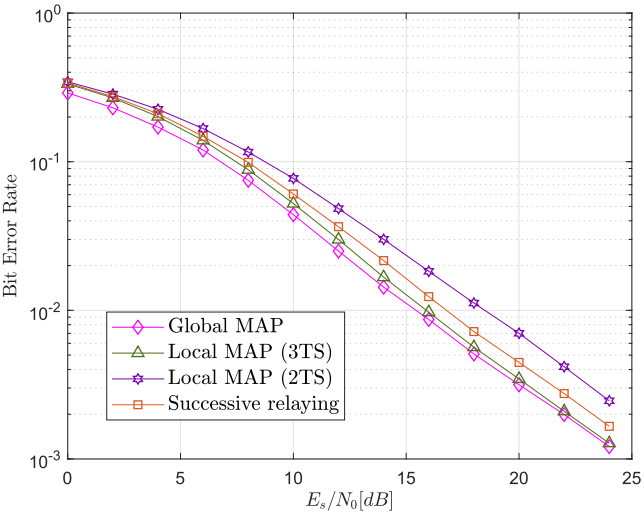

FIGURE 8. BER of the source data at the destination for the case of 4 relays, where QPSK modulation used at the source, and BPSK at the relays. Results are shown for the proposed VFD-DSM protocol with local MAP detection (over 2 and 3 time slots) as well as global MAP detection. The low-complexity demodulator is used in all cases, and the frame length is chosen to be $N = 12$ (targeting $\eta = 93\%$).

MAP detection (2TS) has worse performance than successive relaying; this is due to fact that for a given E_s/N_0, QPSK has a higher symbol error probability than BPSK which leads to a higher rate of incorrect relay activation/inactivation. On the other hand, VFD-DSM with local MAP detection (3TS) and global MAP detection provide a gain of 0.9 dB and 1.3 dB respectively over successive relaying at a BER of 10^{-2}. This shows that even for nonbinary constellations, the VFD-DSM protocol has an advantage of enhancement of the source data detection quality as well as an increased throughput due to the transmission of the relays' data. Note that in the case of this modulation choice ($M_s = 4$, $M_r = 2$), the frame length $N = 12$ was chosen, which represents the optimal choice for

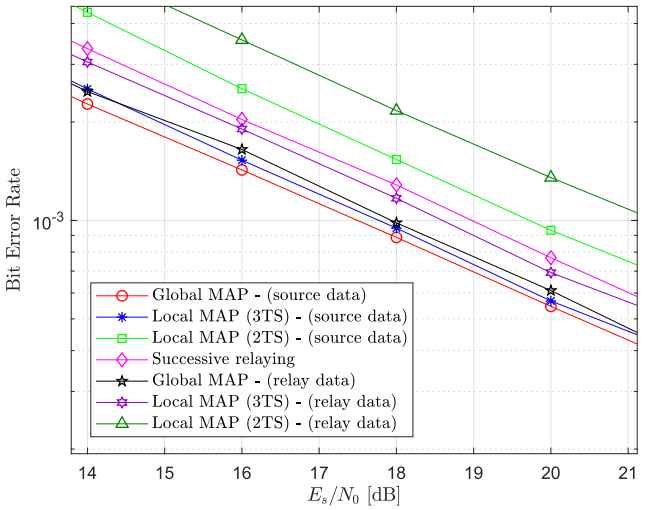

FIGURE 9. BER of source and relay data at the destination for channel geometry G2 and low-complexity demodulators. BPSK is used at both source and relays, and the frame length is $N = 12$.

a system targeting $\eta = 93\%$ of the asymptotic throughput (using (29) and (30) as illustrated in Fig. 5).

D. ROBUSTNESS AGAINST CHANNEL GEOMETRY

In this subsection, we consider a second node geometry (called G2) where both relay nodes lie at the centre point between the source and destination (although not a practical scenario, this is a commonly used as a test case for cooperative protocols). Our model assumes a path loss exponent of 2, so that for the second geometry (called G2), $\sigma^2_{SD} = 1$ while $\sigma^2_{SR_r} = \sigma^2_{R_rD} = 4$ for $r = 1, 2$. The BER performance of the proposed VFD-DSM protocol is compared with that of successive relaying in Fig. 9; here the low-complexity versions of demodulators have been considered. It can be seen that similarly to the case for geometry G1, the BER for the source data is slightly better for global MAP detection than for local MAP detection (3TS), while both of these have a significant gain over that of successive relaying. The BER performance for the relay data shows a similar consistency regarding the relative performance of the different detectors. These results indicate that the performance gains of VFD-DSM are robust against variations in the channel geometry. Again, the throughput advantage of VFD-DSM is implicit in the figure, since for successive relaying the relays only retransmit the source data and there is thus no BER curve for relay data.

VI. CONCLUSION

In this paper, the distributed spatial modulation protocol has been generalized to provide virtual full-duplex operation. Two detection methods were proposed for use at the destination, using a local and a global application of the MAP principle for joint symbol detection. For both local and global MAP detection methods, a low-complexity demodulator which assumes error-free demodulation at the relays was proposed, as well as an error-aware demodulator which

takes into the account the demodulation error probability at the relays. The impact of frame length on the error rate and the system throughput were analysed, and it was shown how to choose the optimal frame length in order to achieve a desired target fraction η of the asymptotic throughput. The proposed detection algorithms were compared in terms of computational complexity and performance. Simulation results indicate that the proposed VFD-DSM protocol and associated detectors exhibit an improved BER performance compared to the state-of-the-art full-duplex relaying technique of successive relaying, especially for the case of error-aware detection. This comes in addition to a significant throughput advantage, since in contrast to successive relaying, in VFD-DSM the relays are able to also transmit their own data in the relaying phase.

ACKNOWLDEGMENT

This paper was presented at the Proceedings of the IEEE Wireless Communications and Networking Conference (WCNC), Barcelona, Spain, April 15–18, 2018.

REFERENCES

[1] E. Biglieri, R. Calderbank, A. Constantinides, A. Goldsmith, A. Paulraj, and H. V. Poor, *MIMO Wireless Communications*. New York, NY, USA: Cambridge Univ. Press, 2007.

[2] M. Di Renzo, H. Haas, and P. M. Grant, "Spatial modulation for multiple-antenna wireless systems: A survey," *IEEE Commun. Mag.*, vol. 49, no. 12, pp. 182–191, Dec. 2011.

[3] P. Yang, M. Di Renzo, Y. Xiao, S. Li, and L. Hanzo, "Design guidelines for spatial modulation," *IEEE Commun. Surveys Tuts.*, vol. 17, no. 1, pp. 6–26, 1st, Quart., 2015.

[4] J. Jeganathan, A. Ghrayeb, and L. Szczecinski, "Spatial modulation: Optimal detection and performance analysis," *IEEE Commun. Lett.*, vol. 12, no. 8, pp. 545–547, Aug. 2008.

[5] R. Y. Mesleh, H. Haas, S. Sinanovic, C. W. Ahn, and S. Yun, "Spatial modulation," *IEEE Trans. Veh. Technol.*, vol. 57, no. 4, pp. 2228–2241, Jul. 2008.

[6] M. Di Renzo, H. Haas, A. Ghrayeb, S. Sugiura, and L. Hanzo, "Spatial modulation for generalized MIMO: Challenges, opportunities, and implementation," *Proc. IEEE*, vol. 102, no. 1, pp. 56–103, Jan. 2014.

[7] P. Yang, B. Zhang, Y. Xiao, B. Dong, S. Li, M. El-Hajjar, and L. Hanzo, "Detect-and-forward relaying aided cooperative spatial modulation for wireless networks," *IEEE Trans. Commun.*, vol. 61, no. 11, pp. 4500–4511, Nov. 2013.

[8] Y. Yang and S. Aissa, "Information-guided transmission in decode-and-forward relaying systems: Spatial exploitation and throughput enhancement," *IEEE Trans. Wireless Commun.*, vol. 10, no. 7, pp. 2341–2351, Jul. 2011.

[9] R. Mesleh and S. S. Ikki, "Performance analysis of spatial modulation with multiple decode and forward relays," *IEEE Wireless Commun. Lett.*, vol. 2, no. 4, pp. 423–426, Aug. 2013.

[10] S. Narayanan, M. Di Renzo, F. Graziosi, and H. Haas, "Distributed spatial modulation for relay networks," in *Proc. IEEE 78th Veh. Technol. Conf.*, Sep. 2013, pp. 1–6.

[11] S. Narayanan, M. D. Renzo, F. Graziosi, and H. Haas, "Distributed spatial modulation: A cooperative diversity protocol for half-duplex relay-aided wireless networks," *IEEE Trans. Veh. Technol.*, vol. 65, no. 5, pp. 2947–2964, May 2016.

[12] A. Shehni and M. F. Flanagan, "Network coded distributed spatial modulation for relay networks," in *Proc. 25th Int. Conf. Telecommun. (ICT)*, St. Malo, France, Jun. 2018, pp. 70–75.

[13] I. Krikidis, H. A. Suraweera, P. J. Smith, and C. Yuen, "Full-duplex relay selection for amplify-and-forward cooperative networks," *IEEE Trans. Wireless Commun.*, vol. 11, no. 12, pp. 4381–4393, Dec. 2012.

[14] I. Krikidis, H. A. Suraweera, S. Yang, and K. Berberidis, "Full-duplex relaying over block fading channel: A diversity perspective," *IEEE Trans. Wireless Commun.*, vol. 11, no. 12, pp. 4524–4535, Dec. 2012.

[15] Z. Ding, I. Krikidis, B. Rong, J. S. Thompson, C. Wang, and S. Yang, "On combating the half-duplex constraint in modern cooperative networks: Protocols and techniques," *IEEE Wireless Commun.*, vol. 19, no. 6, pp. 20–27, Dec. 2012.

[16] Y. Ding, J. K. Zhang, and K. M. Wong, "Ergodic Channel capacities for the amplify-and-forward half-duplex cooperative systems," *IEEE Trans. Inf. Theory*, vol. 55, no. 2, pp. 713–730, Feb. 2009.

[17] J.-S. Han, J.-S. Baek, S. Jeon, and J.-S. Seo, "Cooperative networks with amplify-and-forward multiple-full-duplex relays," *IEEE Trans. Wireless Commun.*, vol. 13, no. 4, pp. 2137–2149, Apr. 2014.

[18] L. Song, Y. Li, and Z. Han, "Resource allocation in full-duplex communications for future wireless networks," *IEEE Wireless Commun.*, vol. 22, no. 4, pp. 88–96, Aug. 2015.

[19] A. Nosratinia, T. E. Hunter, and A. Hedayat, "Cooperative communication in wireless networks," *IEEE Commun. Mag.*, vol. 42, no. 10, pp. 74–80, Oct. 2004.

[20] J. N. Laneman, D. N. C. Tse, and G. W. Wornell, "Cooperative diversity in wireless networks: Efficient protocols and outage behavior," *IEEE Trans. Inf. Theory*, vol. 50, no. 12, pp. 3062–3080, Dec. 2004.

[21] J. N. Laneman and G. W. Wornell, "Distributed space-time-coded protocols for exploiting cooperative diversity in wireless networks," *IEEE Trans. Inf. Theory*, vol. 49, no. 10, pp. 2415–2425, Oct. 2003.

[22] L. Xu, J. Wang, H. Zhang, and T. A. Gulliver, "Performance analysis of IAF relaying mobile D2D cooperative networks," *J. Franklin Inst.*, vol. 354, no. 2, pp. 902–916, Jan. 2017.

[23] S.-N. Hong and G. Caire, "Virtual full-duplex relaying with half-duplex relays," *IEEE Trans. Inf. Theory*, vol. 61, no. 9, pp. 4700–4719, Sep. 2015.

[24] S.-N. Hong, I. Marić, D. Hui, and G. Caire, "Multihop virtual full-duplex relay channels," in *Proc. IEEE Inf. Theory Workshop (ITW)*, Jerusalem, Israel, Apr./May 2015, pp. 1–5, .

[25] L. Bahl, J. Cocke, F. Jelinek, and J. Raviv, "Optimal decoding of linear codes for minimizing symbol error rate (Corresp.)," *IEEE Trans. Inf. Theory*, vol. 20, no. 2, pp. 284–287, Mar. 1974.

[26] A. Shehni and M. F. Flanagan, "Virtual full-duplex distributed spatial modulation with SER-optimal and suboptimal detection," in *Proc. IEEE Wireless Commun. Netw. Conf. (WCNC)*, Barcelona, Spain, Apr. 2018, pp. 1–6.

[27] A. Shehni, S. Narayanan, and M. F. Flanagan, "A virtual full duplex distributed spatial modulation technique for relay networks," in *Proc. IEEE 27th Annu. Int. Symp. Pers., Indoor, Mobile Radio Commun. (PIMRC)*, Valencia, Spain, Sep. 2016, pp. 1–6.

[28] T. Oechtering and A. Sezgin, "A new cooperative transmission scheme using the space-time delay code," in *Proc. ITG Workshop Smart Antennas*, Mar. 2004, pp. 41–48.

[29] S. Yang and J.-C. Belfiore, "On slotted amplify-and-forward cooperative diversity schemes," in *Proc. IEEE Int. Symp. Inf. Theory*, Jul. 2006, pp. 2446–2450.

[30] B. Rankov and A. Wittneben, "Spectral efficient protocols for half-duplex fading relay channels," *IEEE J. Sel. Areas Commun.*, vol. 25, no. 2, pp. 379–389, Feb. 2007.

[31] Y. Hu, K. H. Li, and K. C. Teh, "An efficient successive relaying protocol for multiple-relay cooperative networks," *IEEE Trans. Wireless Commun.*, vol. 11, no. 5, pp. 1892–1899, May 2012.

[32] R. Zhang, "On achievable rates of two-path successive relaying," *IEEE Trans. Commun.*, vol. 57, no. 10, pp. 2914–2917, Oct. 2009.

[33] F. R. Kschischang, B. J. Frey, and H.-A. Loeliger, "Factor graphs and the sum-product algorithm," *IEEE Trans. Inf. Theory*, vol. 47, no. 2, pp. 498–519, Feb. 2001.

[34] H. Chen, R. G. Maunder, and L. Hanzo, "A survey and tutorial on low-complexity turbo coding techniques and a holistic hybrid ARQ design example," *IEEE Commun. Surveys Tuts.*, vol. 15, no. 4, pp. 1546–1566, 2013.

[35] M. Di Renzo, M. Iezzi, and F. Graziosi, "On diversity order and coding gain of multisource multirelay cooperative wireless networks with binary network coding," *IEEE Trans. Veh. Technol.*, vol. 62, no. 3, pp. 1138–1157, Mar. 2013.

[36] M. D. Renzo, M. Iezzi, and F. Graziosi, "Error performance and diversity analysis of multi-source multi-relay wireless networks with binary network coding and cooperative MRC," *IEEE Trans. Wireless Commun.*, vol. 12, no. 6, pp. 2883–2903, Jun. 2013.

AMIR SHEHNI received the B.Sc. degree in electrical engineering (with emphasis on power engineering) from Azad University, Najafabad, Iran, and the M.Sc. degree in electrical engineering (with emphasis on radio communication) from the Blekinge Institute of Technology (BTH) with final thesis co-supervised at the Chalmers University of Technology, Sweden. He is currently pursuing the Ph.D. degree in electronic engineering with University College Dublin (UCD), Ireland. He has some years of industrial experiences as a power and instrumentation engineer in companies such as Agahan and Pars Ghodrat. His research interests include wireless communications, signal processing, information theory, and applied mathematics.

MARK F. FLANAGAN (M'03–SM'10) received the B.E. and Ph.D. degrees in electronic engineering from University College Dublin, Ireland, in 1998 and 2005, respectively. From 1998 to 1999, he was a Project Engineer with Parthus Technologies Ltd. From 2006 to 2008, he held postdoctoral research fellowship positions with the University of Zurich, Switzerland; the University of Bologna, Italy; and The University of Edinburgh, U.K. In 2008, he was appointed as an SFI Stokes Lecturer in electronic engineering with University College Dublin, where he is currently an Associate Professor. In 2014, he was a Visiting Senior Scientist with the German Aerospace Center, Institute of Communications and Navigation, under a DLR-DAAD Fellowship. His research interests include information theory, wireless communications, and signal processing. He has served on the technical program committees of several IEEE international conferences. He is currently a Senior Editor of the IEEE COMMUNICATIONS LETTERS.